NONLINEAR BUCKLING BEHAVIOUR OF CFRP REINFORCED THIN-WALLED STEEL CYLINDERS UNDER LATERAL PRESSURE

Krishna Kumar BHETWAL[1], Seishi YAMADA[2] , Yukihiro MATSUMOTO[3] and Genki SADAOKA[4]

[1]Member of JSCE, PhD Student, Dept. of Architecture and Civil Eng.,
Toyohashi University of Technology, (Toyohashi, Tempaku-ku, 441-8580, Japan)
E-mail:b085605@edu.imc.tut.ac.jp
[2]Member of JSCE and AIJ, Professor, Dept. of Architecture and Civil Eng.,
Toyohashi University of Technology, (Toyohashi, Tempaku-ku, 441-8580, Japan)
E-mail:yamada@ace.tut.ac.jp
[3]Member of JSCE and AIJ, Asst. Prof., Dept. of Architecture and Civil Eng.,
Toyohashi University of Technology, (Toyohashi, Tempaku-ku, 441-8580, Japan)
E-mail:y-matsum@ace.tut.ac.jp
[4]Member of AIJ, Graduate Student, Dept. of Architecture and Civil Eng.,
Toyohashi University of Technology, (Toyohashi, Tempaku-ku, 441-8580, Japan)
E-mail:g115502@edu.tut.ac.jp

This study deals with the buckling behaviour of thin-walled steel cylindrical shells subjected to the lateral pressure and the effect of the carbon fibre reinforcement polymer (CFRP) on it, when they are reinforced externally and internally. A nonlinear numerical experiment has been performed in this study and presents a novel way of strengthening thin-walled steel cylindrical shells during lateral pressure in which application of a small amount of the CFRP composite can increase the buckling strength effectively, when they are coated from the both side with the veneers of the CFRP. On the previous study, it has been pointed out that the CFRPs, when they are applied to the thin-walled cylindrical shells under compression have complex buckling behaviour which is very sensitive to initial geometric imperfections. In the case of the orthotropic CFRP material, the angles and dispositions of fibre orientations, as well as the magnitudes of any imperfections, have been suggested to affect the buckling behaviour. In this study, to obtain the valuable information for the design of the FRP based hybrid structural elements having the complex buckling collapse behaviour, the nonlinear numerical experiments have been carried out for the CFRP laminated reinforced thin-walled steel cylinders under lateral pressure. Also, in this research, the best angle of fibre orientations while CFRPs are sandwiched with steel in the case of laterally pressurized cylindrical shells has been studied and its action on the buckling strength as well as on the associated buckling mode, amplitude and imperfection modes adopting the symmetrical model for the analysis.

Key Words : *Carbon fibre reinfored polymer*, *Cylindrical shell*, *Lateral pressure*, *Nonlinear numerical experiment*, *Initial imperfection*

1. INTRODUCTION

Fibre reinforced polymer (FRP) composites, comparatively new and revolutionary class of composite material manufactured from fibres and resins, serves the constant demands of the society and is an effective material to achieve the impressive gains over high strength, light weight and safe economical structures. For years, civil engineers have been in search for alternatives to steel and its alloys to combat the high costs of repair and maintenance of steel structures damaged by corrosion and heavy use. Carbon fibre reinforced polymer (CFRP) is an alternate source of effective material which has the benefit of high strength to weight ratios along with corrosion resistance. In addition, several researches have shown that these CFRPs are ideally suited for short-term retrofits and long-term rehabilitations because of having merit of the ease of handling during construction[1] with excellent durability in aggressive environments. Therefore; these composites are particularly suitable for the design of bridges, large span structural members, aerospace components and pressure vessels. Since steel shells are considerably stiffer than the CFRP composites, strengthening them requires expensive high-strength fibres and thus, this procedure has been generally deemed not advantageous. Despite this fact, El Damatty et al. [2] have shown both experimentally and numerically, that glass fibre (GFRP) plates can be used to enhance the load-carrying capacity. Nevertheless, there is no doubt that CFRP are, of course, expensive and less processable than GFRP, but has predominant advantage of high stiffness. However, these composites have drawback having relatively lower stiffness driven by CFRP's. Consequently, serviceability rather than strength limit states tend to provide the controlling influence on design constraint in the context of thin-walled shell structures. So that the required buckling strength could not be obtained for the shells constructed just from CFRP only. In this case, a novel way to improve this drawback of CFRP would be, jointly use with thin-walled steel plates. So that strength properties of the steel could be increased and possibility of corrosion inside the marine environments also would be vanished because the carbon fibres are chemically inert and have low surface energy. In this study, CFRP laminated thin-walled steel cylinders under lateral pressure are treated with nonlinear numerical experiment to obtain the valuable information for the design of CFRP based hybrid structural elements and discusses the influence of CFRP reinforcements to increase the load carrying capacity of the thin-walled metallic structures having complex buckling collapse behaviour. In the case of CFRP material, the angles and dispositions of fibre orientations, as well as the magnitudes of any imperfections, have been suggested to affect the buckling behaviour[3].Since, the mechanical behaviour of CFRP shells is much dependent upon the fibre orientation [4,5], the relative fibre orientation has been given priority for the analysis for $\theta = 0^\circ$ and $\theta = 90^\circ$. Also, in our previous study, it has been shown that for the axially compressed thin-walled CFRP reinforced steel cylinders, depending upon the imperfections, buckling modes as well as buckling load carrying capacity differs and this capacity varies with the adopted reinforcement together with the angle of fibre orientation[6]. Therefore, in this paper, a nonlinear numerical experiment has been performed in the case of laterally pressurized CFRP reinforced steel cylinders to determine how best to alter the angle of fibre orientation.

2. METHOD OF ANALYSIS

2.1. CFRP Lamina and CFRP Reinforced Steel Lamination

As shown in Fig. 1 a section of thin-walled CFRP reinforced steel cylinder, which is termed as FSF-model (fibre steel fiber) is considered in which x-y denotes the coordinate of thin cylindrical shell

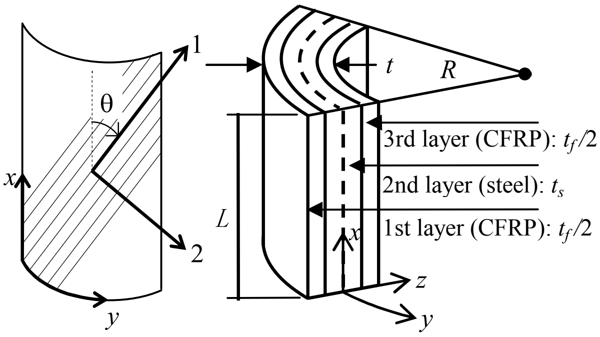

Fig. 1: Section of FSF thin cylindrical shell with angle of fibre orientation θ

and 1-2 denotes the coordinates along fibre direction. The material constants are obtained by using Halpin-Tsai equation [7] as

$$\begin{Bmatrix} E_1 = E_F V_F + E_P V_P, \mu_{12} = \mu_F V_F + \mu_P V_P, \\ \mu_{21} = \dfrac{E_2}{E_1}\mu_{12} \end{Bmatrix} \tag{1}$$

In Eq.1 subscript F and P relate to fibre and polymer, respectively. E_1 represent elastic coefficient and E_F and E_P as elastic constants for fibre and polymer, respectively. Also, V_F and V_P represent volume fraction for fibre and polymer and μ_{12} and μ_{21} as Poisson's ratios. In Eq.1 E_2 is the elastic coefficient normal to the fibre and calculated as $E_2 = E_P\left(1+\xi\eta V_F\right)/\left(1-\eta V_F\right)$ Parameters ξ is taken as ξ =2 and $\eta = \left\{\left(E_F/E_P\right)-1\right\}/\left\{\left(E_F/E_P\right)+\xi\right\}$. Again, the shear modulus of elasticity G_{12} can be calculated as $G_{12} = G_P\left(1+\xi\eta V_F\right)/\left(1-\eta V_F\right)$ and the associated parameter ξ for the calculation of G_{12} is taken as $\xi = 1+40\,V_F^{10}$ and η for the calculation of G_{12} is

$\eta = \{(G_F / G_P) - 1\} / \{(G_F / G_P) + \xi\}$. The resulting transformed linear elastic constants after the transformation of the linear elastic constants from the principal material fibre directions to a global *x-y* coordinate is as below

$$\begin{Bmatrix} \bar{\sigma}_x \\ \bar{\sigma}_y \\ \bar{\sigma}_{xy} \end{Bmatrix} = \begin{bmatrix} \bar{Q}_{11} & \bar{Q}_{12} & 0 \\ \bar{Q}_{12} & \bar{Q}_{22} & 0 \\ 0 & 0 & \bar{Q}_{66} \end{bmatrix} \begin{Bmatrix} \bar{\varepsilon}_x \\ \bar{\varepsilon}_y \\ 2\bar{\varepsilon}_{xy} \end{Bmatrix} = \left[\bar{Q}_{ij}\right] \begin{Bmatrix} \varepsilon_x \\ \varepsilon_y \\ 2\varepsilon_{xy} \end{Bmatrix} + z\left[\bar{Q}_{ij}\right] \begin{Bmatrix} \kappa_x \\ \kappa_y \\ 2\kappa_{xy} \end{Bmatrix} \tag{2}$$

Where,
$Q_{11} \equiv E_1 / (1 - \mu_{12}\mu_{21}), Q_{12} \equiv \mu_{12} E_1 / (1 - \mu_{12}\mu_{21}),$
$Q_{22} \equiv E_2 / (1 - \mu_{12}\mu_{21})$ and $Q_{66} \equiv G_{12}$,($\bar{\sigma}_x, \bar{\sigma}_y, \bar{\sigma}_{xy}$) and ($\bar{\varepsilon}_x, \bar{\varepsilon}_y, \bar{\varepsilon}_{xy}$) are the principal stress and strain components associated with *x-y* plane, and similarly, (ε_x, ε_y, ε_{xy}) and (κ_x, κ_y, κ_{xy}) are the corresponding membrane and bending strains on the middle plane of the shell respectively. Also, by integrating the whole thickness of lamina, the membrane and bending stress resultant matrices can be obtained as

$$\begin{Bmatrix} n_x \\ n_y \\ n_{xy} \end{Bmatrix} = \left[A_{ij}\right] \begin{Bmatrix} \varepsilon_x \\ \varepsilon_y \\ 2\varepsilon_{xy} \end{Bmatrix} + \left[B_{ij}\right] \begin{Bmatrix} \kappa_x \\ \kappa_y \\ 2\kappa_{xy} \end{Bmatrix}$$
$$\begin{Bmatrix} m_x \\ m_y \\ m_{xy} \end{Bmatrix} = \left[B_{ij}\right] \begin{Bmatrix} \varepsilon_x \\ \varepsilon_y \\ 2\varepsilon_{xy} \end{Bmatrix} + \left[D_{ij}\right] \begin{Bmatrix} \kappa_x \\ \kappa_y \\ 2\kappa_{xy} \end{Bmatrix} \tag{3}$$

Where, (n_x, n_y, n_{xy}) and (m_x, m_y, m_{xy}) are the total membrane and bending stress resultants respectively. Similarly, A_{ij}, B_{ij} and D_{ij} are respectively the membrane, membrane bending coupling and bending stiffness respectively. From Eq. (3) the constitutive relation for the laminated plate can be calculated as

$$\begin{Bmatrix} n_x \\ n_y \\ n_{xy} \\ m_x \\ m_y \\ m_{xy} \end{Bmatrix} = \begin{bmatrix} A_{11} & A_{12} & 0 & B_{11} & B_{12} & 0 \\ A_{12} & A_{22} & 0 & B_{12} & B_{22} & 0 \\ 0 & 0 & A_{66} & 0 & 0 & B_{66} \\ B_{11} & B_{12} & 0 & D_{11} & D_{12} & 0 \\ B_{12} & B_{22} & 0 & D_{12} & D_{22} & 0 \\ 0 & 0 & B_{66} & 0 & 0 & D_{66} \end{bmatrix} \begin{Bmatrix} \varepsilon_x \\ \varepsilon_y \\ 2\varepsilon_{xy} \\ \kappa_x \\ \kappa_y \\ 2\kappa_{xy} \end{Bmatrix} \tag{4}$$

In the present study, symmetric laminations are adopted. So that, all the components of B_{ij} will be zero.

2.2 Nonlinear Imperfection Analysis

For an imperfect CFRP reinforced thin-walled steel cylinders the change in the total potential energy, consequent upon the application of lateral pressure p may be written as

$$\Pi = \Pi_m + \Pi_b + \Pi_\lambda \tag{5}$$

where Π_m are the membrane strain energies, Π_b are the bending energies and Π_λ are the external pressure.

$$\Pi_m = \frac{1}{2}\int_0^{2\pi R}\int_0^L \left(n_x\varepsilon_x + n_y\varepsilon_y + 2n_{xy}\varepsilon_{xy}\right) dxdy$$
$$\Pi_b = \frac{1}{2}\int_0^{2\pi R}\int_0^L \left(m_x\kappa_x + m_y\kappa_y + 2m_{xy}\kappa_{xy}\right) dxdy \tag{6}$$
$$\Pi_\lambda = -p\int_0^{2\pi R}\int_0^L w dxdy$$

In Eq. 6, (n_x, n_y, n_{xy}) and (m_x, m_y, m_{xy}) are calculated using the constitutive relation for the laminated plate as shown in Eq. 4.

To get the strain-displacement relationship Donnel-Mushtari-Vlasov type is adopted for the deformations from the initial imperfections w^0 as

$$\kappa_x = -\frac{\partial^2 w}{\partial x^2}, \quad \kappa_y = -\frac{\partial^2 w}{\partial y^2}, \quad \kappa_{xy} = -\frac{\partial^2 w}{\partial x \partial y}$$
$$\varepsilon_x = \frac{\partial u}{\partial x} + \frac{\partial w^0}{\partial x}\frac{\partial w}{\partial x} + \frac{1}{2}\left(\frac{\partial w}{\partial x}\right)^2,$$
$$\varepsilon_y = \frac{\partial v}{\partial y} - \frac{w}{R} + \frac{\partial w^0}{\partial y}\frac{\partial w}{\partial y} + \frac{1}{2}\left(\frac{\partial w}{\partial y}\right)^2, \tag{7}$$
$$\varepsilon_{xy} = \frac{1}{2}\left(\frac{\partial u}{\partial y} + \frac{\partial v}{\partial x} + \frac{\partial w^0}{\partial x}\frac{\partial w}{\partial y} + \frac{\partial w^0}{\partial y}\frac{\partial w}{\partial x} + \frac{\partial w}{\partial x}\frac{\partial w}{\partial y}\right)$$

End boundaries are assumed to be supported in such a way as to conform to the classical simple support, corresponding with the conditional expression as

$$w = 0, \partial^2 w/\partial x^2 = 0, \partial u/\partial x = 0, v = 0 \text{ at } x = 0, L \tag{8}$$

The linear sum of bi-harmonic function that satisfy the above boundary condition, the displacement functions u, v and w as

$$u = \sum_{i=0,b,2b,3b} \sum_j^{J_i^u} u_{i,j}\cos(iy/R)\cos(j\pi x/L)$$
$$v = \sum_{i=b,2b,3b} \sum_j^{J_i^v} v_{i,j}\sin(iy/R)\sin(j\pi x/L) \tag{9}$$
$$w = \sum_{i=0,b,2b} \sum_j^{J_i^w} w_{i,j}\cos(iy/R)\sin(j\pi x/L)$$

where, $u_{i,j}$, $v_{i,j}$ and $w_{i,j}$ are the amplitudes of each harmonic function; i and j are the circumferential full-wave and the longitudinal half-wave number, respectively. The initial geometric imperfection is taken to consist of a harmonic of

$$w^0 = w^0_{b,f}\cos(by/R)\sin(f\pi x/L) \tag{10}$$

in which b and f represent the circumferential full-wave and longitudinal half-wave number, respectively.

3. RESULTS AND DISCUSSIONS

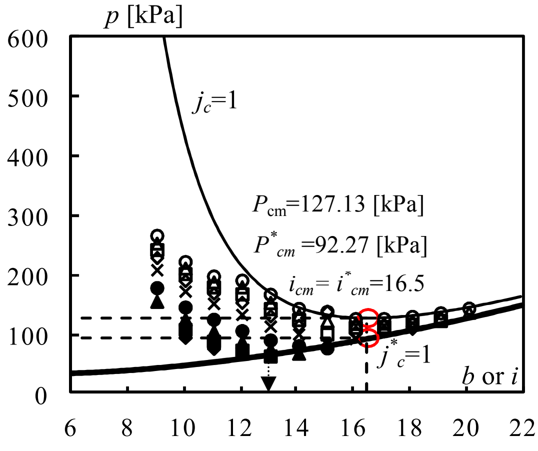

Fig.(2a): for model S

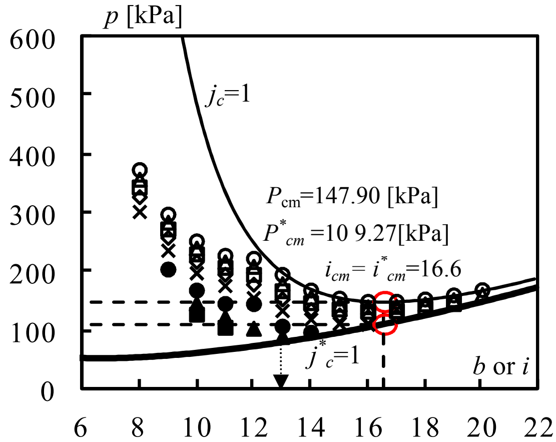

Fig.(2b): for model FSF-1, with θ=0°

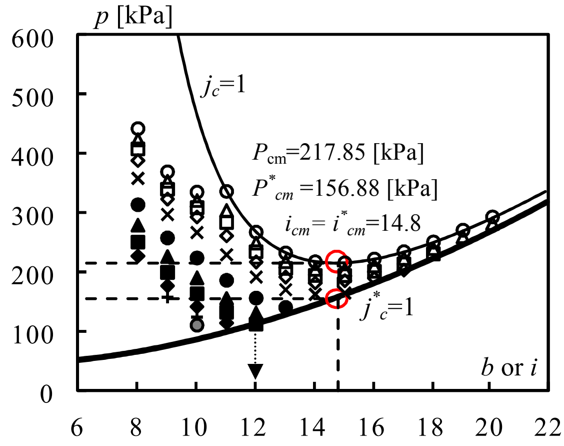

Fig.(2c), for model FSF-1 with θ=90°

Fig:(2a), (2b) and (2c); Load Spectra for model S, FSF-1, θ=0° and FSF-1, θ=90°

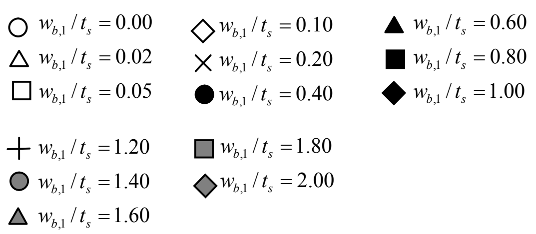

For the analysis of laterally pressurised reinforced shells, steel and FRP's are laminated with constant steel with wall thickness of t_s = 4mm as shown in Fig.1 and the adopted geometrical parameters are L/R= 0.512 and R/t_s= 405. Also, t_f represents the thickness of carbon fibre ranging the thickness of fibre from 0 to t_s. Similarly, Model S indicates for steel with no reinforcement and FSF-1 indicates for steel with reinforcement 1 mm CFRP on each side. While, Young's moduli for steel, fibre and polymer are taken as E_s = 205GPa, E_F = 235GPa, E_P = 3.5GPa, and Poisson's ratios for steel, fibre and polymer are μ_s = 0.3, μ_F = 0.3 and μ_P = 0.34, respectively.

Figs.(2a), (2b) and (2c), are the outcome of nonlinear imperfection analysis, linear buckling analysis and the reduced stiffness (RS) analysis with the horizontal axis as circumferential full wave number i for model S (t_f = 0mm) and FSF-1 (t_f = 1mm) model with angle of fibre orientation 0° and 90°, respectively. The linear buckling loads with varying longitudinal half-wave number j are defined as $P_{cm.j}$. Then the corresponding circumferential full-wave number is obtained as $i_{cm}(j)$. After that, its RS critical load associated with $i_{cm}(j)$ is calculated as $P^*_{cm,j}$. Consequently, from all the calculated $P^*_{cm,j}$, the minimum value can be selected as defining the RS criterion[8)] P^*_{cm} as depicted on figures.But in this paper, predicting the lower bound by RS buckling load and its impact will not be discussed briefly, only the influence of nonlinear numerical experiment of larger imperfections having a form (b,f) = (13,1) with amplitude $(w^0_{13,1})/t$=0.8 for model S, (b,f) = (13,1) with amplitude $(w^0_{13,1})/t$=0.6 for model FSF-1 having an angle of fibre orientation 0° and (b,f) = (12,1) for model FSF-1 with amplitude $(w^0_{13,1})/t$=0.8 having an angle of fibre orientation 90°, where the minimum nonlinear buckling loads exhibits and are observed to produce buckling loads that are lower than P^*_{cm} associated with the mode $(i^*_{cm},1)$. What is fascinating about the nonlinear results are that despite the shape of initial imperfection, $(w^0_{12,1})$, the incremental mode at buckling, at least when imperfection amplitudes are large, is dominated by wave form having considerably shortened circumferential and axial wave lengths. For the case of FSF-1 model and θ= 90° shown in Fig. 5b, for example, the incremental mode at buckling for the large imperfection $w^0_{12,1}/t$ = 0.8, has through a process of modal coupling reached localised shapes closer to that associated with (i,j) = (12, 1.82).

Figs. 3a and 3b are the result of nonlinear numerical experiment for model S, b=13 where the minimum

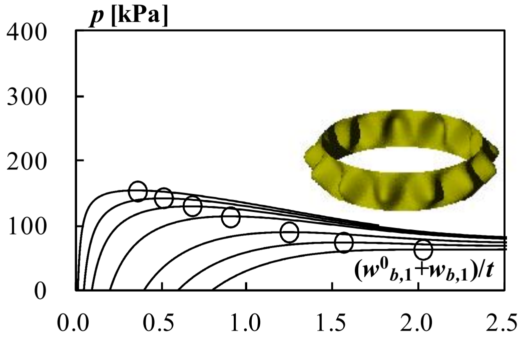

Fig.3a: Load versus displacement curves for model S

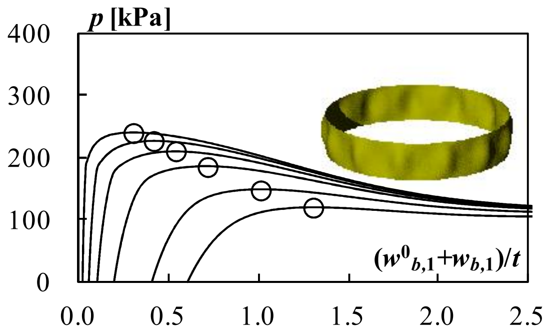

Fig.4a: Load versus displacement curves for model FSF-1, θ = 0°

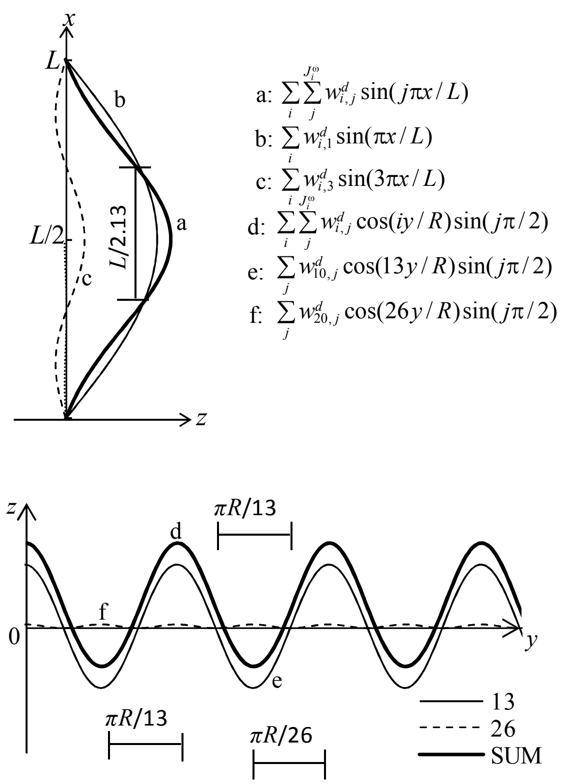

Fig.3b: Incremental wave forms at buckling points for model S

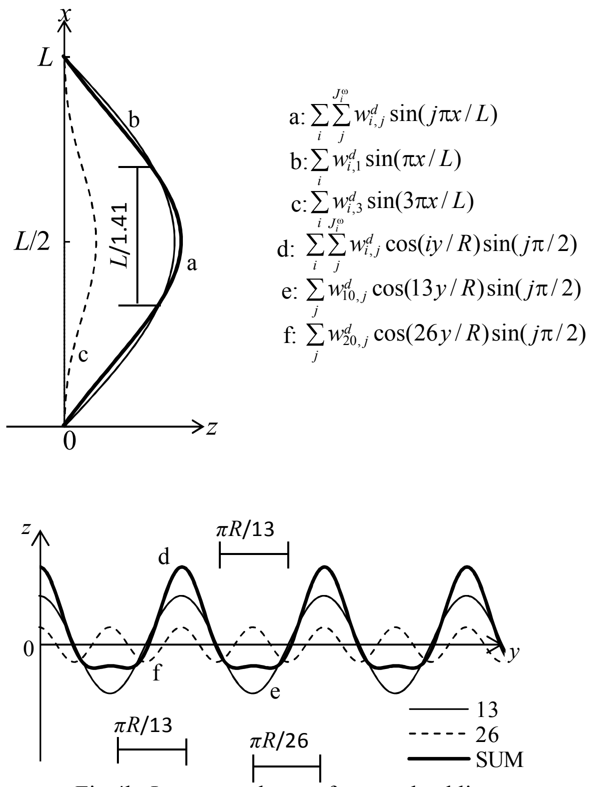

Fig.4b: Incremental wave forms at buckling points for model FSF-1 with θ=0°

nonlinear buckling load occurs. Fig. 3a is the load versus displacement curves with increamental displacement at the buckling mode in the case of b=13 and Figs. 3b are the incremental cirumferential at x=L/2 and axial y=0 wave forms at the buckling points. Similarly, Fig. 4a is the load versus displacement curves with increamental displacement at the buckling mode in the case of circumferential full wave number b= 13, for model FSF-1 with an angle of fibre orientation θ=0° and Figs. 4b are the incremental cirumferential at x=L/2 and axial y=0 wave forms at the buckling points. Figs. 5a and 5b have the same explanations for the same model as Figs.4a and 4b but with an angle of fibre orientation θ=90° and b=12.

While compairing the Figs. 3a, 4a, and 5a, it can be understood that the buckling load carrying capacity is higher for reinforced condition (Figs.,4a and 5a) and attains maximum strength in the case of θ=90° for all the amplitudes and this capacity will be the highest as we decrease the amplitude. Similarly, the outward increamental displacement at the buckling points is sharp during nonreinforced condition (Model S) and if we look for the reinforced condition (FSF-1 model) in both cases of θ=0° and θ=90°, it is determined that the sharpness of outward increamental displacement goes on decreasing and attains the least value during angle of fibre orientation at θ=90° exhibiting the considerable

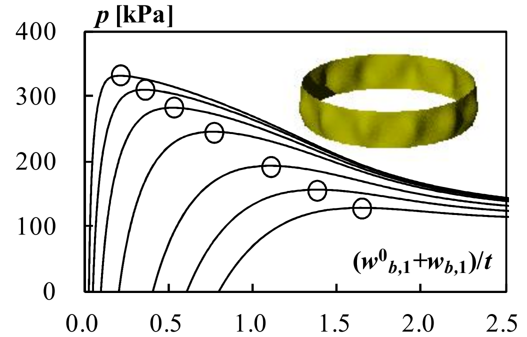

Fig.5a: Load versus displacement curves for model FSF-1, θ = 90°

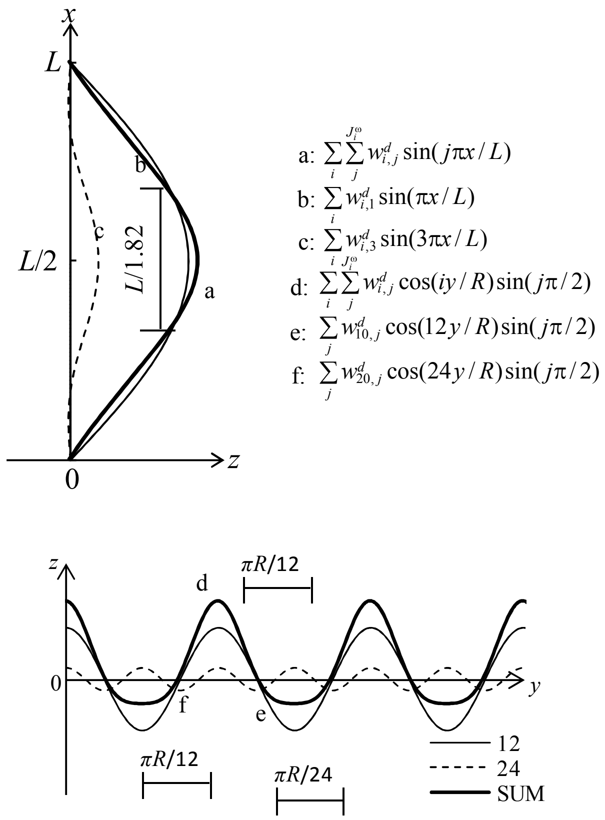

Fig.5b: Incremental wave forms at buckling points for model FSF-1, θ= 90°

dependence upon the angle of fibre orientation, on the other hand, the buckling loads for large imperfections also remarkably shows load dependence upon the angle of fibre orientation within it. For this mechanism, it can be stated that CFRP reinforcements act as the stiffners from the both sides reducing the axial and circumferential outward increamental displacement and thus load carrying capacity of the proposed model is increased. Again, Figs. 3b, 4b and 5b shows the typical significant changes in mode at buckling as compared with the form of initial imperfection in the case of axial (y=0) and circumferential (x=L/2). These all figures shows the process of modal coupling which reached the localized shapes closer to that associated with the (i,j)= (13, 2.13) for model S, (13, 1.41) for model FSF-1 with θ=0° and (12, 1.82) for model FSF- with θ =90°, respectively.

4. CONCLUSIONS

In this paper, nonlinear numerical experiments have been carried out for the CFRP laminated reinforced thin-walled steel cylinders under lateral pressure and found that with the CFRP reinforcement, load carrying capacity of the thin-walled steel cylinders will be increased tremendously but depends upon the angle of fibre orientation. For the symmetrical case of laterally pressurized CFRP reinforced thin-walled steel cylinders, it is best to adjust the angle of fibre orientation at θ=90° to obtain the maximum load carrying capacity. Also, from the analysis it is understood that the influence imperfection is very high for pressurised cylindrical shells.

REFERENCES

1) Moy S. (2001), ICE Design and Practice Guides, *FRP composites life extension and strengthening of metallic structures.* London (UK), Thomas Telford Publishing.
2) El Damatty, A.A., Abushagur, M., and Youssef, M.A. (2003), "Experimental and analytical investigation of steel beams rehabilitated using GFRP sheets", *Steel & Composite Structures*, Vol.3, issue 6, 421–438.
3) Yamada, S. and Croll, J.G.A. (1999), "Contributions to understanding the behavior of axially compressed cylinders", *J. Applied Mechanics*, ASME, Vol. 66, 299-309.
4) Matsumoto K., Yamada S., Wang H.T. and Croll J.G.A: (2007), "Buckling and reduced stiffness criteria for FRP cylindrical shells under compression", *Proceedings of Asia-Pacific Conference on FRP in Structures,* APFIS 2007, Vol.1, 465-470.
5) K.K., Bhetwal, , Yamada, S. and Yanagida, M. (2009), "Buckling and reduced stiffness analyses of laminated carbon fiber reinforced polymer cylindrical shells", *Proc. of the 7th Japan-Korea Joint Symp. on Composite Materials*, JACM, Kanazawa, p.241-242.
6) K.K, Bhetwal and Yamada, S. (2003), "Effects of CFRP reinforcements on the buckling behaviour of thin-walled steel cylinders under compression", *International Journal of Structural Stabilityand Dynamics*, Vol.12, No.1 (2012), 131-151.
7) Jones, R.M. (1999), *Mechanics of Composite Materials*, Taylor & Francis.
8) Batista, R.C. and Croll, J.G.A. (1979) "A design approach for axially compressed unstiffened cylinders", *Stability Problems in Engineering Structures and Components*, Applied Science, London.